12 Mar 1991, 9:00 am - 10:00 am

Seismic Amplification in the Presence of Geological and Topographic Irregularities

E. Faccioli
Technical University of Milan, Milan, Italy

Proceedings: Second International Conference on Recent Advances in Geotechnical Earthquake Engineering and Soil Dynamics, March 11-15, 1991, St. Louis, Missouri, Paper No. SOA7

Seismic Amplification in the Presence of Geological and Topographic Irregularities

(State of the Art Paper)

E. Faccioli
Professor of Engineering Seismology, Technical University of Milan, Milan, Italy

SYNOPSIS

Following some introductory remarks on the key aspects of seismic site effects evaluation and on new data of special interest from recent earthquakes, the first part of the paper discusses and compares the performance of numerical 2D and 1D models, as well as of simple exact solutions, in problems of local soil response and of topographic amplification. The second part is devoted to the illustration of a very promising computational tool, i.e. the Fourier (or pseudospectral) method, for time-domain analyses of seismic wave propagation in heterogeneous elastic media.

INTRODUCTION

Many of the key problems involved in the determination of site effects on strong earthquake ground motion were recently reviewed by Aki (1988), and as an appropriate starting point for my considerations I will recall his main conclusions:

- Observed areal variations of local amplification typically span over a factor of 10 for frequencies between 1 and 10 Hz, while the change in amplification factor due to variation of incident waves has a standard error (s.e.) of about 2. Hence, meaningful microzonation maps can be constructed, at least in the 1 to 10 Hz frequency range.

- Based on successful comparisons of observations and theory, site effects can be adequately predicted in many realistic situations if one knows input motions, propagation velocity and density of soils, as well as their stratigraphic profile (with surface topography), and the internal damping coefficient.

- Since the modeling required by theoretical predictions is expensive in terms of necessary input and computer time, a realistic approach consists of trying to correlate empirically determined amplification factors with various geotechnical parameters of the site that can be measured relatively easily.

- Except for the obvious case of soil liquefaction (and of other soil failure mechanisms), numerous observations show that amplifications for weak and strong motions are similar to the first order.

Posterior to Aki's review, new data from moderate Pacific coast events of 1988 and 1989 extensively recorded in the valley of Mexico (Mexico City area), as well as from the 1989 Loma Prieta, California earthquake, possibly warrant some adjustments and further distinctions in the previous conclusions. As an example, within the hard ground zone in the valley of Mexico the amplitude of motion from a $M_s \approx 7.0$ distant earthquake can vary by more than a factor of 3, as shown in Fig. 1. This will contribute to enhancing the standard error of the spectral amplification curves for the soft clay zone in the same area, except possibly if such curves are referred to a specific hard ground site. In case the amplitude spread were confirmed for stronger earthquakes, the data of Fig. 1 would also imply that local irregularities (such as topography) capable of causing amplitude variations of a factor of 3 may not be resolvable in the framework of a microzoning study.

Furthermore, for loose saturated soils the similarity between weak and strong motion amplification, well supported by observations on firm soil or rock sites, is at variance with the data of the 1989 Loma Prieta earthquake. This is illustrated in Fig. 2 by the comparison of weak and strong motion spectral ratios from the accelerograph stations of Treasure Island (TRI), located on rock, and Yerba Buena Island (YBI), located on saturated sand or fill less than 3 km apart. It is to be noted that the 5 sec time window chosen for both stations to calculate the main shock spectral ratio precedes what could be interpreted as a symptom of onset of liquefaction in the TRI record (Jarpe et al., 1989). Fig. 2 gives a strong indication that the behavior of soil under TRI during the main shock was non linear, although the amplification is still higher than 2 between 1 and 4 Hz.

Especially in the first part of this paper, I will consider the evaluation of site effects on seismic motions mostly from the viewpoint of the designer, who must often take decisions on the basis of limited information on soil properties and seismic input. Also, in most cases he cannot afford the lengthy and sophisticated calculations required by many 2D models, not to speak of 3D ones. This is not only due to computational costs, but also to difficulties of access to computer codes often developed only for research purposes, or in evaluating their performance.

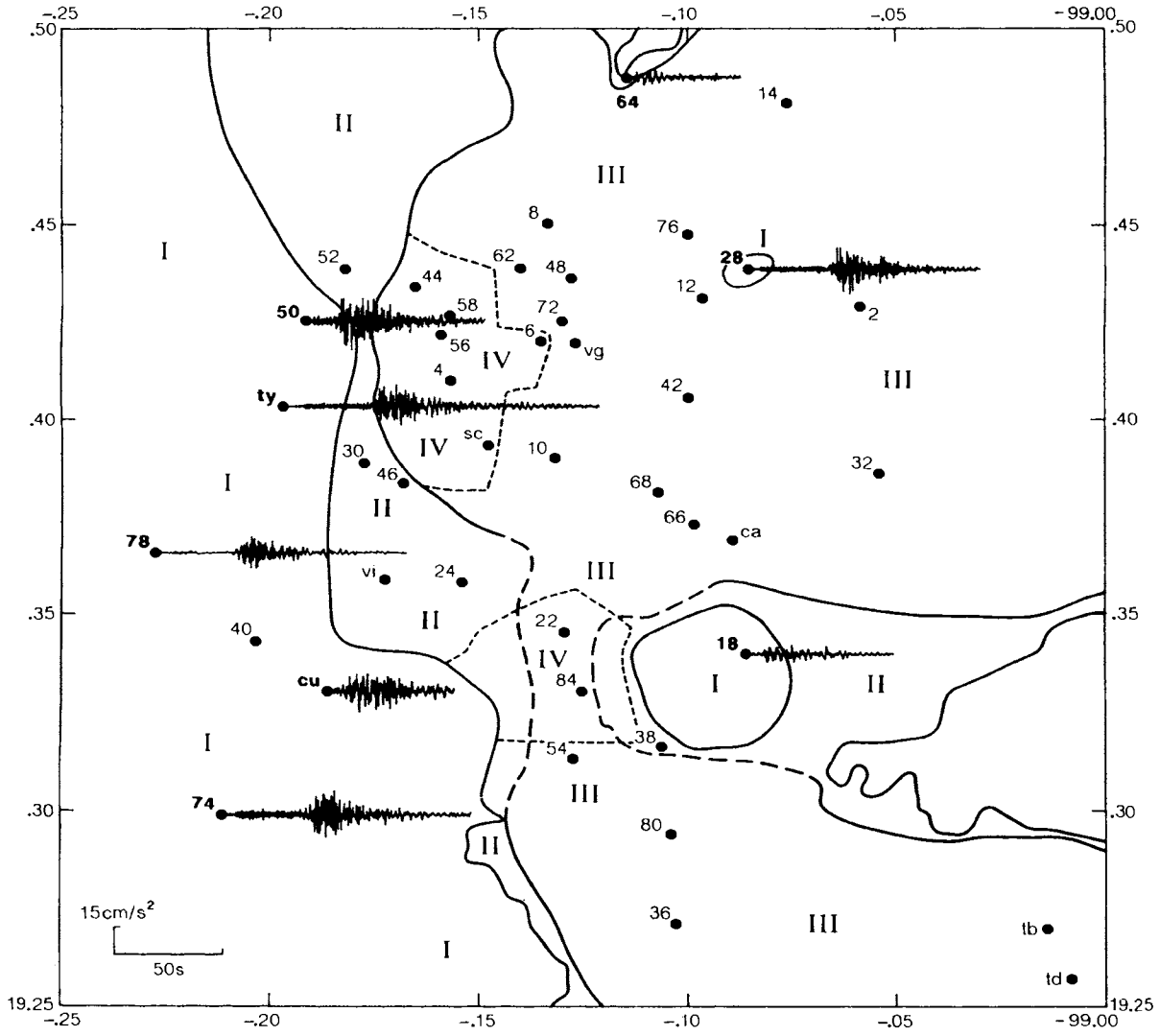

Fig. 1. Valley of Mexico: digital accelerograph stations of the Fundación Barros Sierra local array, shown by dots, with NS components of motion recorded on hard ground during the M_s 7.1, Pacific Coast earthquake of 25.04.89. Zones labeled I ("hills"), II ("transition"), III and IV ("lakebed") are from the geotechnical zoning map included in the 1987 editions of the Mexico City building code. Numbered dots outside zone I indicate the other stations which recorded the earthquake.

In such a perspective, the attention will be focused on the following aspects of seismic site response evaluation:

1. Unexplored implications of 2D vs. 1D modeling approaches;
2. Applicability of simple 2D models to estimate amplification effects due to topography;
3. Difficulties in the selection of appropriate input motions;
4. Illustration of an efficient algorithm for the time-domain analysis of 2D problems for heterogeneous viscoelastic media.

Items 2,3 often recur in the literature on site effects. For instance, attention on item 2 was recently called also by Aki (cit.) while the feasibility of expressing complex amplification effects through a single coefficient, or TEI (= Topography Effects Index), was explored elsewhere (Sánchez-Sesma et al., 1986).

As regards item 4, when 2D site response analyses are needed, earthquake engineers tend to make use of FEM, because they are more familiar with them. However, such methods may not be adequate for certain classes of problems involving strong jumps of material properties, deformable and irregular bottom boundary, or very large dimensions. I believe that in reality there is a need of methods that can be easily implemented by the users, without recurring to large and difficult-to-use computer programs. The last section of this paper is devoted to illustrate the characteristics and potentiality of one such method.

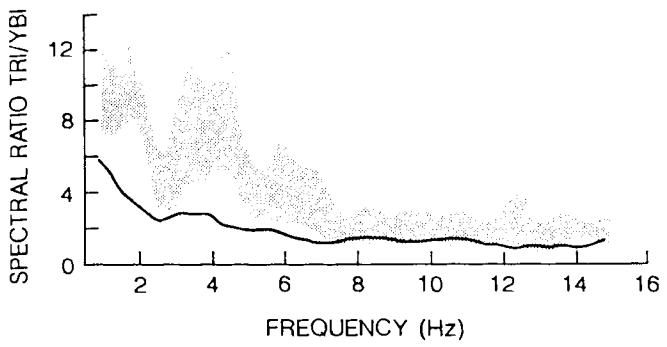

Fig. 2. Relative site response of soft site (TRI) with respect to rock site (YBI) during the 17.10.89 Loma Prieta earthquake and some of its aftershocks. The solid line is the NS spectral ratio for the first 5 sec of the S-wave of main shock, while the shaded band is the 95% confidence region for the NS spectral ratio averaged for 7 aftershocks. After Jarpe et al. (1989).

2D VS. 1D MODELS OF SEISMIC RESPONSE: SOME HITHERTO UNEXPLORED IMPLICATIONS

Effects of spatial fluctuations of material properties

The choice between 2D and 1D seismic soil response models appears to be decided in practice by many engineers in the following way: there is hardly any need of complicating things with 2D models because 1D models usually provide good enough estimates of natural period of vibration, amplification coefficients, and elastic response spectrum at a soil site, provided the stratigraphy and the shear wave velocity β are reasonably well known.

The performances of 1D and 2D methods for viscoelastic soil response have been extensively compared and tested against the data in the case of the soft clay deposits of the valley of Mexico, which constitutes a unique natural laboratory for site effects. Resonant frequencies as a function of the local thickness of clay agree well with the simple one-quarter-wavelength formula (Singh et al., 1988). Also, the response spectrum at some of the accelerograph sites recording the destructive Michoacán earthquake of 19.9.85 is well reproduced by standard 1D models provided one uses in situ measurements of β for the clay and, as an input, the specific record of the seemingly hard site at Ciudad Universitaria, labeled II in Fig.1 (Seed et al., 1988). As shown later on, the choice of this input is quite critical. Similar results, obtained by different 1D models and supported by lower quality instrumental data from previous earthquakes had been reported in previous studies, e.g. by Faccioli and Reséndiz, (1976).

On the other hand, the peak spectral amplifications and the extreme durations of significant motion observed especially in the central and eastern parts of the valley cannot be reproduced by 1D models, and their interpretation can only be attempted by 2D, and possibly 3D models. The complexity of the patterns of ground motion occurring through the valley, which could only be guessed from the scarce data of 1985, is better appreciated for the moderate earthquakes recorded by the dense local arrays installed after 1985. The hard site motions of Fig. 1 can thus be complemented by those recorded on the soft clay of the lakebed zone during the cited earthquake of 25.04.89. Fig. 4 displays the EW acceleration component recorded by a group of stations on the alignment AA' (shown in Fig. 3a), where the gradual increase in clay thickness towards the center of the lake zone is to be noted.

Several factors evidently concur to determine the spatial variations of observed ground motions. The geometries of both the clay

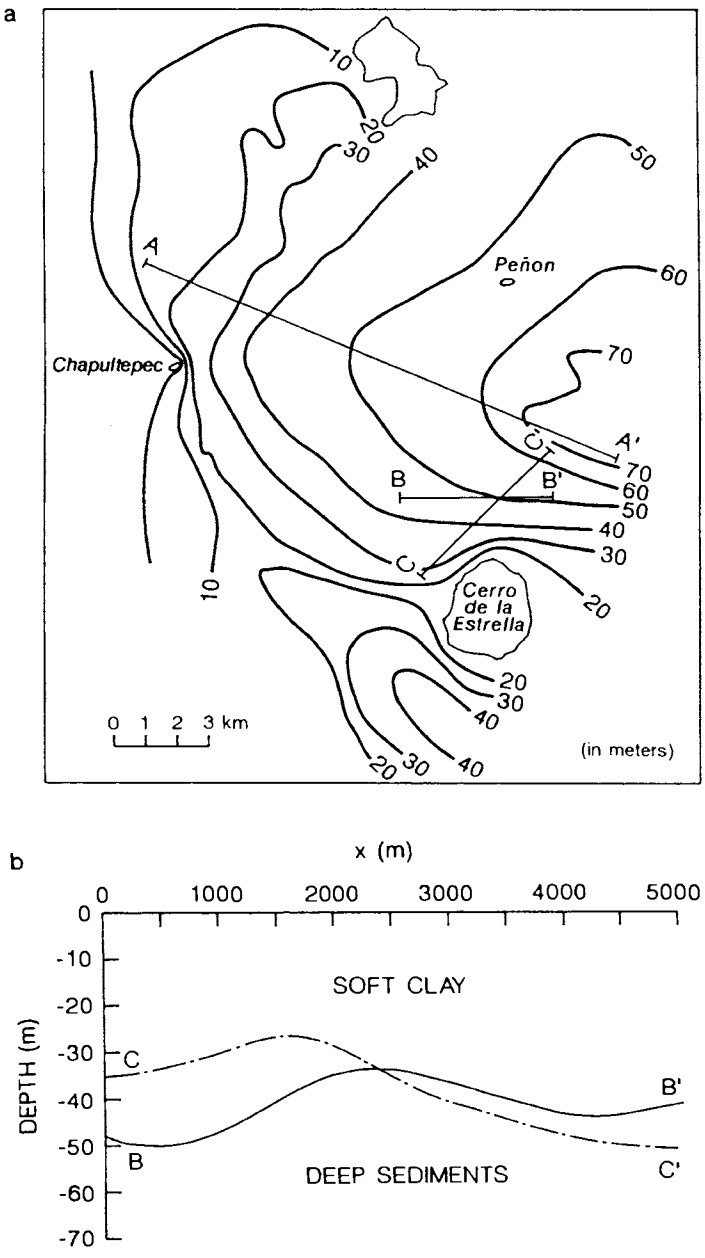

Fig. 3. (a) Thickness contours (in m) of clay lakebed deposits in the valley of Mexico, with the position of some representative cross-sections, shown in (b) and in Fig.4.

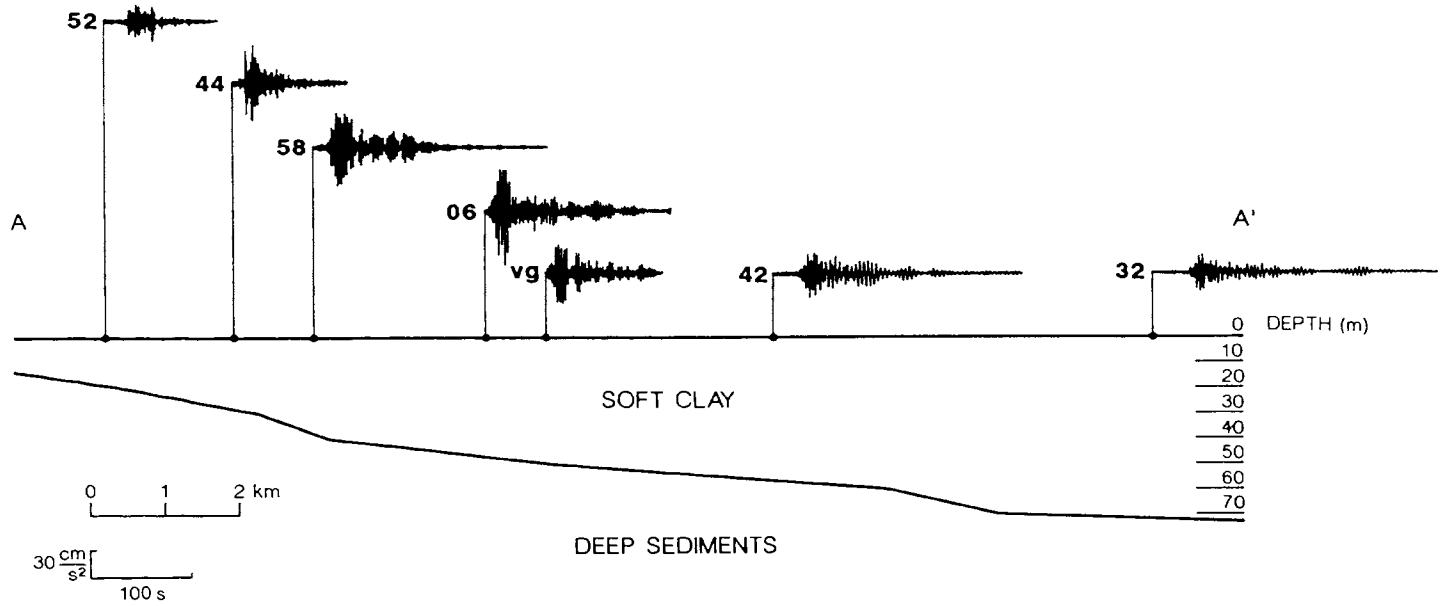

Fig. 4. Representative cross-section of the valley of Mexico clay deposits, located as shown in Fig.3, with NS ground acceleration components recorded on 25.04.89 by stations located along the trace of the cross section (see Fig.1).

lakebed, still poorly known in some parts of the valley, and of the underlying firm sediments, almost entirely unknown, are perhaps the most evident ones, and their effects were investigated by different 2D models (Sánchez-Sesma et al., 1988; Bard et al., 1988; Ohta et al., 1986).

Another cause of potentially strong perturbations stems from spatial variations in the mechanical properties of the surficial soils which can, for simplicity, be limited to the S-wave propagation speed β. It has been shown through 1D analyses that, owing to the strong impedance contrast with the underlying sediments, modest perturbations in the clay β-values produce large changes in the response spectrum at the surface (Seed et al., 1988). Based on the evidence of Fig. 5, appreciable fluctuations of β must exist both in vertical and horizontal direction, and although in situ data are still limited, simple analyses of the spatial variability of β are possible and its influence can be tested in seismic response analyses. Some 2D numerical simulations were performed for this purpose on model of a soft surficial deposit underlain by hard sediments which is not intended to reproduce exactly any specific subsoil cross-section in the valley of Mexico, but rather to investigate the conditions of occurrence of some of the observed ground motion phenomena (Faccioli et al., 1989b).

A similar approach was adopted by Chávez-García and Bard (1989), who studied the influence of random irregularities in the clay/deep-sediments interface on the surface motions. For example, they calculated a s.e. of about 0.3 at the peak of the response spectrum, arising from an interface at a mean depth of40 m, with maximum vertical irregularity of only 20 m and mean wavelength 341 m. For a given earthquake the intrinsic variability of the long period

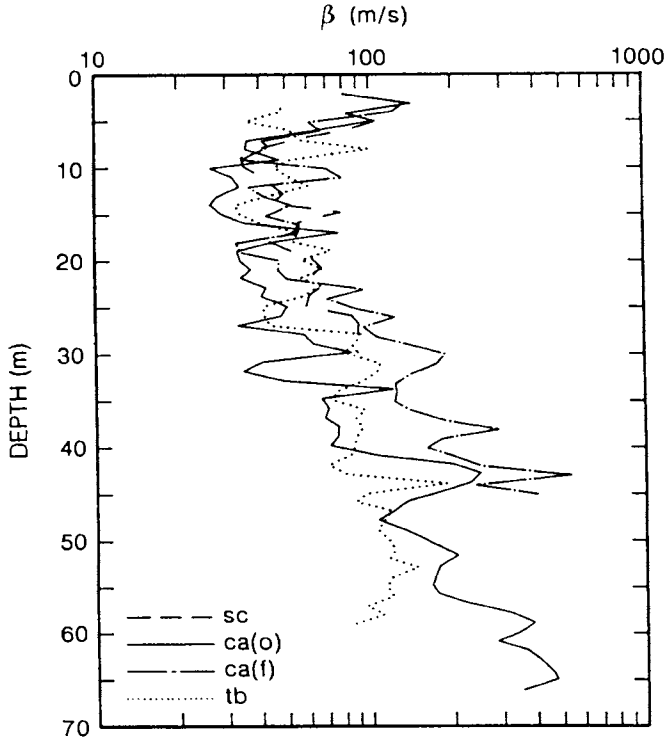

Fig. 5. Profiles of S-wave velocity β measured by the P-S logging technique at the sites of four accelerograph stations, shown in Fig.1. After Jaime (1987).

spectral ordinates on alluvium was also found to be about 30%, based on the SMART 1 array data in Taiwan (Caillot and Bard, 1990).

By a simple correlation analysis on the ensemble of four profiles of β measured at lakebed sites the autocorrelation coefficient in vertical direction was obtained (Fig. 6); velocity fluctuations in the clay are uncorrelated for vertical distances > 2-3 m, which are substantially smaller than the grid step used in computations. Hence, the fluctuations in vertical direction can be treated as white noise in the models. Horizontally, due to lack of data, random fluctuations with a Gaussian autocorrelation function were assumed having a correlation distance a = 250 m. The standard deviation of the fluctuations of β in the clay over four vertical profiles was found to be 28 m/s, whereas the mean values are typically between 50 and 80 m/s.

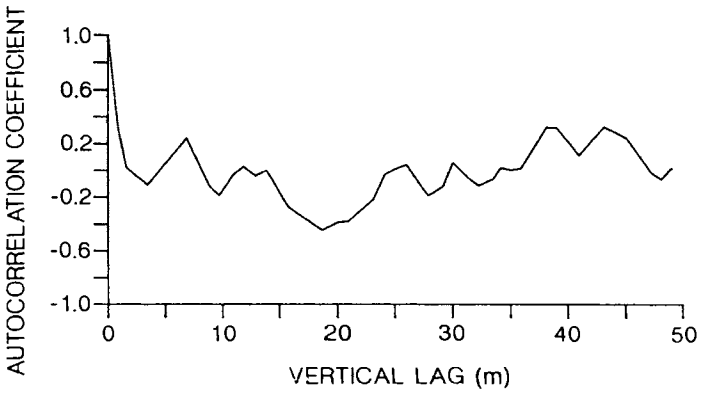

Fig. 6. Autocorrelation coefficient of velocity β vs. vertical lag in the Mexico clay. From Faccioli et al. (1989).

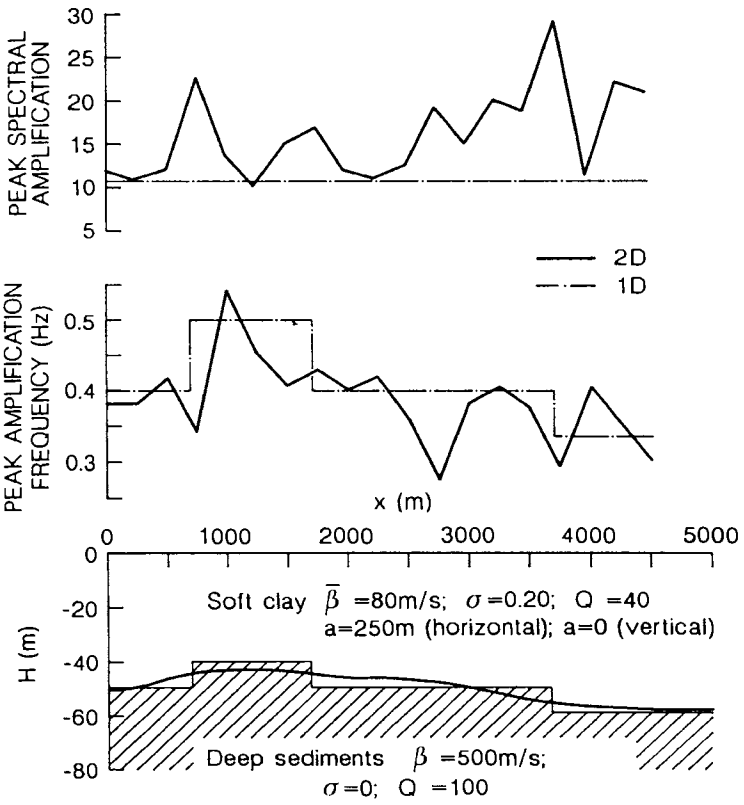

Fig. 7. Artificially generated cross-section of the surficial deposits in the valley of Mexico (bottom) used for 2D analysis of the influence of random fluctuations of β on the seismic response. The results are synthesized in terms of peak spectral amplification (top) and corresponding frequency (middle) as a function of position, and are compared with the prediction of 1D deterministic model.

Based on the actual distribution of clay thickness (see Fig. 3b), a 2D model was constructed having a clay/deep-sediments interface with a Gaussian random shape as illustrated at the bottom of Fig. 7 (shown by straight lines in the same figure is the discretized model approximation). The artificially generated interface resembles those of actual cross sections such as BB' and CC' in Fig. 3b. A mean velocity $\bar{\beta}$ = 80 m/s with a standard deviation of 0.2, was assigned to the clay, whereas a constant value was kept for the deep sediments, as shown in Fig. 7. Intrinsic dissipation with frequency-independent quality factors Q=40 and 100 were assumed for the clay and the deep sediments, respectively.

Spatial grid steps of 10 m (vertically) and 25 m (horizontally), as well as a time step of 0.008 sec were used, and the computations were performed by the pseudospectral method described in a later section. Seismic excitation is in the form of a vertically incident SH displacement impulse consisting of a Ricker wavelet with characteristic frequency f_p = 0.8 Hz.

Partial results of this analysis include displacement synthetics at regular intervals on the surface (Fig. 8), and the spatial distribution of peak spectral amplification (Fig. 7) and of the associated frequency, limited to a single realization of the random fluctuations of β. Hence, although not representative statistically, the results portray the extent of the influence locally exerted by a moderate spatial variability of β on seismic ground response. For instance, the distribution of peak spectral amplification, which mantains a recognizable dependence on the clay thickness not predicted by 1D models, can locally exceed by more than a factor of 2 the 1D values (without fluctuations). The reverberations in the coda of the synthetics of Fig. 8 suggest that local inhomogeneities are trapping the wave energy, and thus cause significant durations of motion to differ by a factor of 3 at some points. The fact that this can occur when the excitation consists of a simple impulse lasting less than 3 sec, suggests that material inhomogeneities may well be one of the main causes of the codas lasting up to 200 seconds observed during distant earthquakes (compare Figs. 1 and 4). Also note in Fig. 7 that the frequency of peak amplification, although it agrees on the average with 1D predictions, can suffer strong local variations, as in the case of the receiver at 2750 m.

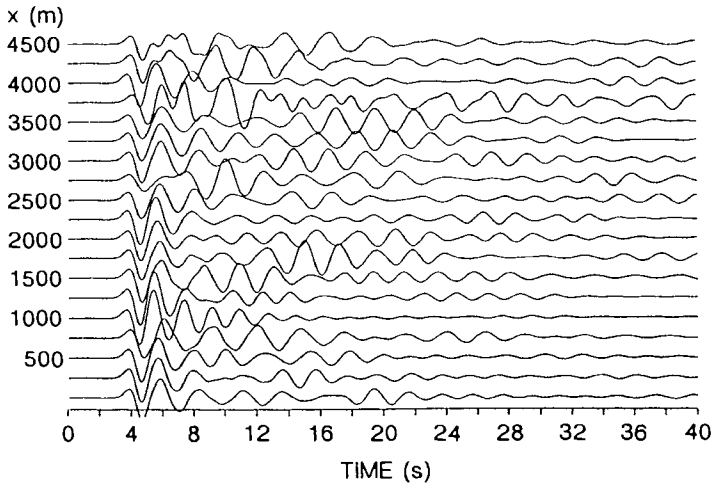

Fig. 8. Displacement synthetics at receivers evenly spaced on the surface of the model at bottom of Fig.7. After Faccioli et al. (1989).

Dynamic soil deformations by 2D and 1D models for seismic pile analysis

Results immediately useful for design purposes can sometimes be obtained from exact solutions for simple analytical models. I illustrate one example, involving as a significant problem the determination of seismic soil deformations to be used as a "kinematic" load for up to 60 m deep reinforced concrete piles and diaphragms. These constitute the foundations of expressway bridge piers at a moderately seismic site of NE Italy, characterized by the (simplified) subsoil cross-section of Fig. 9. The expressway runs parallel to the edge of a broad valley, where the surficial silty soil deposit takes the shape of an irregular wedge, approximated for simplicity by a regular one with a 30° dip angle from the horizontal.

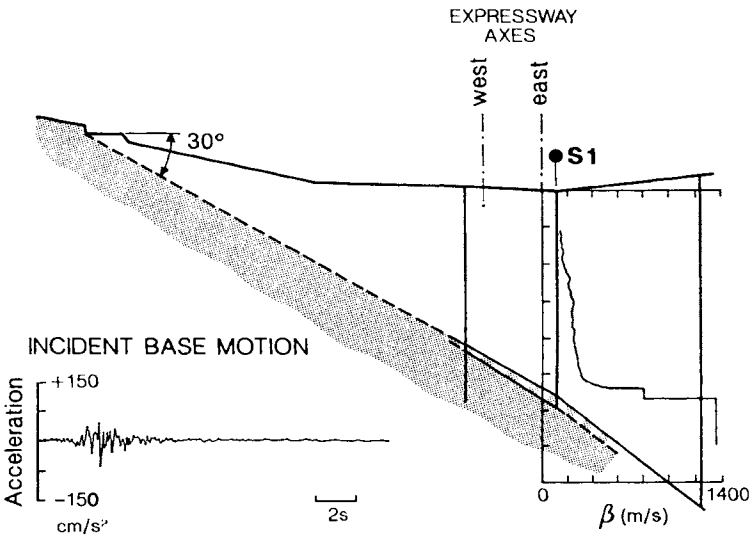

Fig. 9. Cross-section of edge of an alluvial valley near Belluno, NE Italy, including values of S-wave velocity β measured by cross-hole survey in borings S1, close to the axis of a new expressway bridge.

The low values of β of the silt deposit are illustrated by the profile measured at point S1, also shown in Fig. 9. The sloping bedrock underneath consists of faulted limestone with β = 1300 m/s, having on top a thin layer af altered marl (ignored in the seismic analysis). Shown at bottom left of Fig. 9 is one scaled real accelerogram (from the 1976 Friuli earthquakes), taken to represent the incident earthquake at the base of the deposit.

To compute soil displacements along a vertical in the wedge use was made of the simple exact solution for the surface motion found by Sánchez-Sesma et al. (1988) for dip angles from horizontal equal to $\pi/2N$ (N = 1,3,5,...) and SH excitation with rigid base. This was extended first to an arbitrary point within the wedge. Fig. 10 displays the rays and geometrical quantities of interest for the case N = 3. For an incident motion at the base having the form v_0 f(t), where f(t) is an arbitraty time function, the out-of-plane displacement at an arbitrary point x,z within a wedge of dip angle ϕ and velocity β is found to be

$$\frac{v(x,z;t)}{v_0} = \left[\sum_{j=0}^{M-1} (-1)^j \left[f(t-t_{(z1)j}) + f(t-t_{(z2)j})\right]\right] + (-1)^M f(t-t_{z3}) \qquad (1)$$

where

$$t_{(z1)j} = \frac{\left(x + \frac{z}{tg\theta_j}\right)}{\beta} \cos\theta_j - \frac{z}{\beta \sin\theta_j}$$

$$t_{(z2)j} = \frac{\left(x - \frac{z}{tg\theta_j}\right)}{\beta} \cos\theta_j + \frac{z}{\beta \sin\theta_j}$$

$$t_{(z3)} = (1/\beta)\left(\frac{z}{tg\,\phi} - \frac{z}{tg\,\theta_{M-1}}\right)\cos\theta_{M-1} + \frac{z}{\beta \sin\theta_{M-1}} + \frac{x - (z/tg\phi)}{\beta}$$

and

$$\theta_j = (N - 2j - 1)\pi/2N \,, \quad M = (N-1)/2.$$

When ϕ = 18° and 30°, $t_{z3} = x/\beta$. As noted by Sánchez-Sesma et al., the solution is simply a sum of plane waves simultaneously departing from the origin with angles $\pm\theta_j (j = 0,1,..,M)$.

The appropriate sum terms in (1) were further modified through a reflection coefficient to account for an elastic base, and a dissipative convolution operator (Kjartansson, 1979) was also applied to introduce hysteretic damping in the soil. Horizontal displacement histories relative to the base were computed at several points along the vertical S1 in Fig. 9 using a velocity β = 100 m/s (reduced value, compatible with earthquake-induced soil strains) and a damping coefficient of 0.07 in the wedge, while β = 1300 m/s was retained for the base

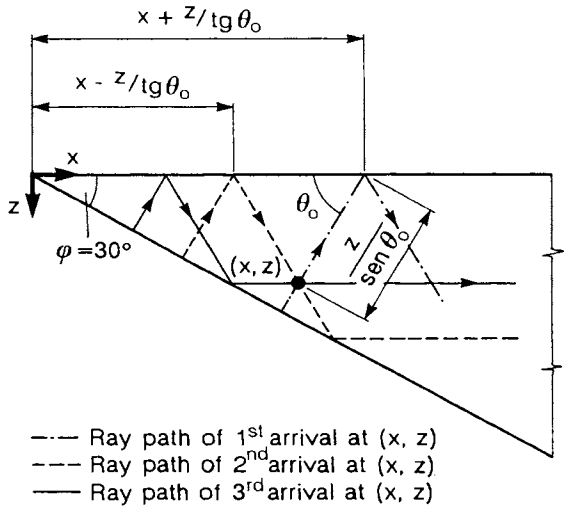

Fig.10. Geometry of horizontal 30° wedge, with seismic ray paths contributing to the motion at an arbitrary point.

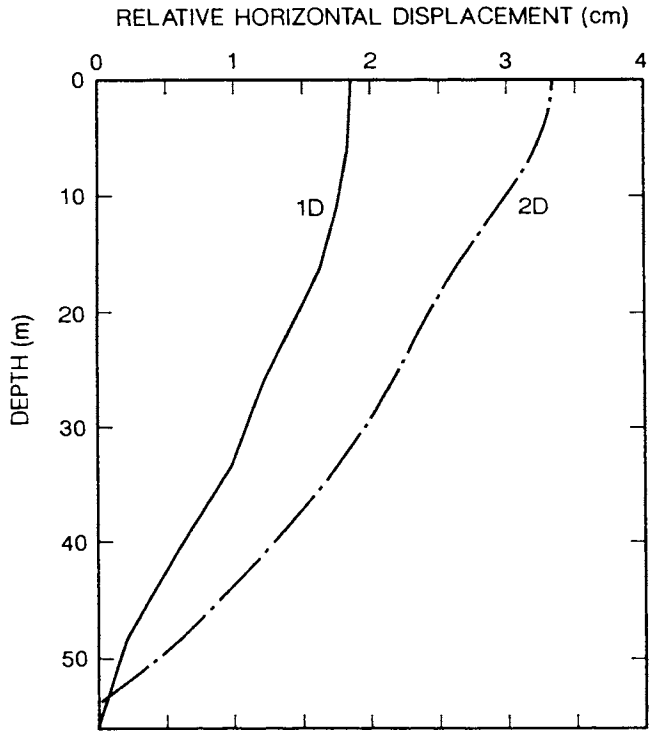

Fig.11. Comparison of horizontal soil displacement (relative to the base) computed by the 2D wedge model of Fig.10 and by 1D model, using the acceleration time history of Fig.9 as base motion.

material. The soil displacement profile to be used for pile design is shown in Fig. 11 and is obtained from the previous time histories by selecting the instant when horizontal deflections appear to be most severe. The 2D profile for the 30° dipping layer is compared in Fig. 11 with that yielded by a 1D linear viscoelastic analysis on a single homogeneous layer 55 m thick resting on an elastic half space, having the same properties used for the 2D solution and subject to the same excitation.

The comparison indicates that a 1D evaluation of seismic soil deformations is in this case not appropriate, since the relative displacements and the ensuing curvatures that the soil motions would impose on a pile in the 2D case are significantly more severe. This is not wholly unexpected considering the difference in lateral confinement effects arising in the wedge and in the layer.

TESTING THE APPLICABILITY OF SIMPLE 2D MODELS TO ESTIMATE TOPOGRAPHIC AMPLIFICATION EFFECTS.

Aki (cit.) already noted that useful estimates of topographic amplification can be obtained through simple exact solutions for elementary irregularities, such as the frequency-independent amplification value $2/\nu$ occurring at the vertex of a wedge with angle $\nu\pi$ excited by SH waves in the direction of its axis. A real topographic profile could thus be approximated as sketched in Fig. 12a, and an estimate of the amplification of SH waves motion at point 2 with respect to point 1 would simply be ν_1/ν_2, provided the two points are sufficiently far apart. For angles representative of severe morphology changes, such as $\phi_2 \simeq 60°$ and $\phi_1 \simeq 180°$, the amplification would be about 3, which confirms the previous

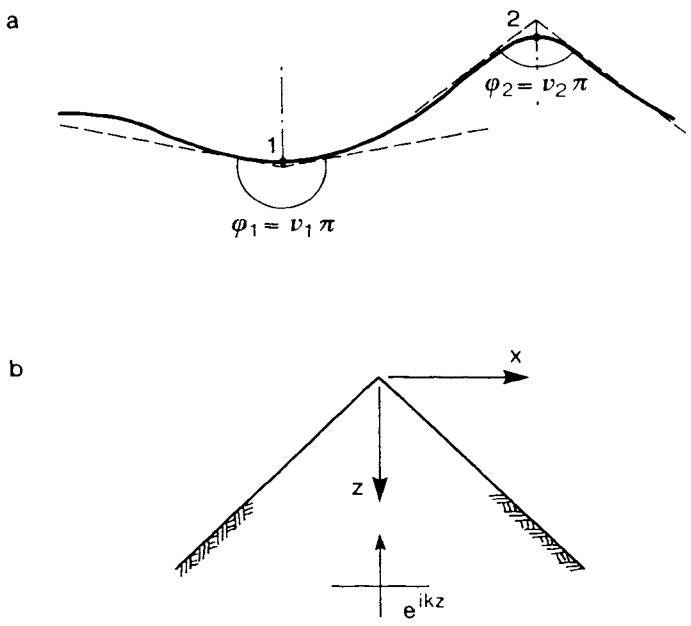

Fig.12. (a) Topographic irregularity, shown by solid line, with wedge approximations at points 1 and 2. (b) Geometry of infinite wedge excited by plane seismic waves in the direction of its axis.

suggestion that the topographic site effects are presumably of the same order as the regional variability of motions on hard ground. Amplification in simple irregularities due to incident P-SV waves, although somewhat larger in the average than for SH waves is roughly of the same magnitude.

Additional results of interest can be obtained from the complete solutions of harmonic SH and SV waves for the 90° and 120° wedge, see Sánchez-Sesma (1990). Referring to Fig. 12b, for a vertically incident arbitrary SH wave $f(t + z/\beta)$, the response on the surface of the 90° wedge ($x = \pm z$) is simply

$$v(z,t) = 2\,[f(t - z/\beta) + f(t + z/\beta)]. \qquad (2)$$

For vertically incident SV waves, some elaboration of the results by Sánchez-Sesma yields the following expression for the displacement perpendicular to the surface

$$s=(u^2 + w^2)^{\frac{1}{2}} = \sqrt{2}\,[f(t-z/\beta) - f(t+z/\beta)]. \qquad (3)$$

which shows that the vertex motion is zero.

For the 120° wedge excited by SH waves, one gets

$$v = 2f(t + z/\beta) + f(t - 2z/\beta) \qquad (4)$$

while for SV waves an exact solution was found only for a Poisson coefficient equal to 1/4, having the same expression as (2) for the displacement component u on the surface, while w = 0.

The previous exact solutions were computed using 5 horizontal acceleration recordings of recent Italian earthquakes (Table I) to represent the incident wavefield. In each case, the peak acceleration obtained from (2), (3) and (4) as a function of z/β was normalized by the corresponding peak acceleration at the vertex.

TABLE I. Accelerograms used for topographic amplifications of wedges.

Event	M_L	Station	Comp.	Epi-central dist. km	a_{max} cm/s^2
Friuli 6.5.76 (20:00)	6.3	Tolmezzo	NS EW	25	360 317
Friuli 15.9.76 (09:21)	6.0	S. Rocco	NS	15	313
Irpinia 23.11.80	6.5	Sturno Mercato S.S.	EW EW	35 50	305 136

The mean and the s.e. of the 5 normalized peak values as a function of z/β are illustrated for the 120° wedge in Fig. 13. The mean peak acceleration has a roughly constant value of about 0.7 for $z/\beta \geq 0.05$. In the SV case the amplitude at the vertex is 4 times that of the incident wave, or 2 times the amplitude at the surface of the half-space. Hence, the mean amplification on the side of a wedge-shaped mountain with respect to a flat surface is estimated as 0.7/0.5 = 1.4, except near the top.

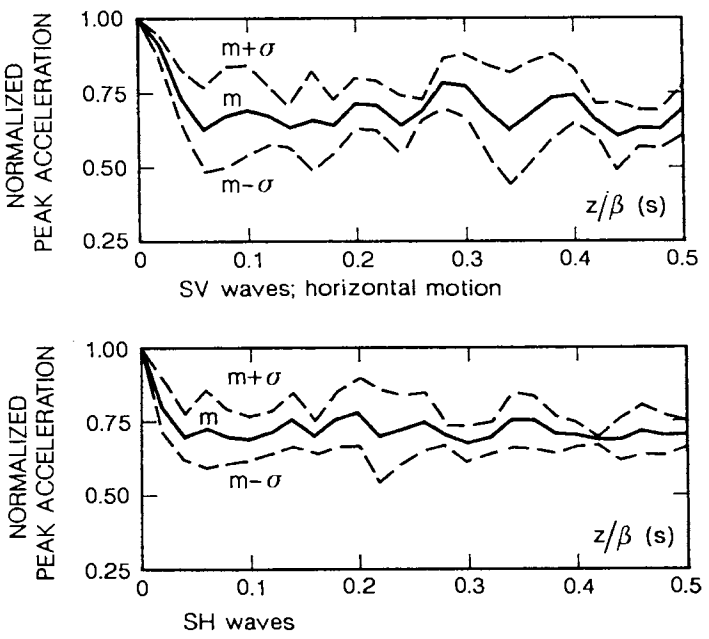

Fig.13. Normalized peak acceleration for 120° wedge; the mean curve (m) and standard deviation ($m \pm \sigma$) intervals are calculated using the five acceleration time-histories of Table I as an input.

By the same reasoning, the mean amplification coefficient for SH waves would be about 1.1. According to (4) and (2), no interference occurs if

$$3\ z/\beta > D_0 \qquad \text{(SH waves)} \qquad (5)$$

$$2\ z/\beta > D_0 \qquad \text{(SV waves)} \qquad (6)$$

where D_0 is the duration of the incident motion. Duration values satisfying (5) and (6) evidently exceed the range of z/β values of Fig. 13, in the case of moderate and strong earthquakes. On the other hand, constructive interference arising from multiple reflections increases rapidly close to the vertex, i.e. for $z/\beta \leq 0.05$ s.

We feel that the foregoing results from time-domain analysis may have more interest for engineering applications than the Fourier spectral ratios, which strongly depend on frequency and position, and therefore are more difficult to use. Even so, validation by experimental observations remains greatly desirable.

Among the data that might be appropriate for this purpose are those from the local strong-motion array in Matsuzaki, Japan (PWRI, 1986). Because of the regrettable policy of the institution operating the array, the data are not made available to the research community (Tokida, 1989); a report by Jibson (1987) lists however the peak accelerations recorded during 5 different earthquakes by stations 1 to 5 of the array, which are located on a ridge, with a maximum elevation difference of about 170 m as shown in Fig. 14. The magnitude and distance of the earthquakes are not reported, but the peak

horizontal values range from a few gal (at st. 5) to slightly over 100 gal (st. 1). Plotted in Fig. 14, for the five earthquakes, are the mean values and s.e. bars of the peak acceleration as a function of absolute elevation, normalized with respect to the corresponding peak values at st. 1.

The mean amplification at st. 1 with respect to the base is about 3, and while the mean curve qualitatively agrees with the mean curves of Fig. 13, the increase of observed amplification between st. 3 and st. 1 far exceeds the calculated one near the vertex. The discrepancy can perhaps be interpreted by noting that the convex angle at the base of the irregularity generates diffraction, which tends to reduce the peak values with respect to the case of an infinite slope. The comparison is of limited significance, however, since the ridge at the Matsuzaki array can hardly be approximated by an infinite 120° wedge. Lack of published information on the earthquake characteristics, as well as on the actual 3D geometry of the topographic irregularity, unfortunately precludes more detailed numerical modeling. Nevertheless, the data seem to confirm the magnitude of the amplification predicted by exact solutions at the most elevated point of the irregularity and, quantitatively, the steep increase in motion amplitude occurring near it.

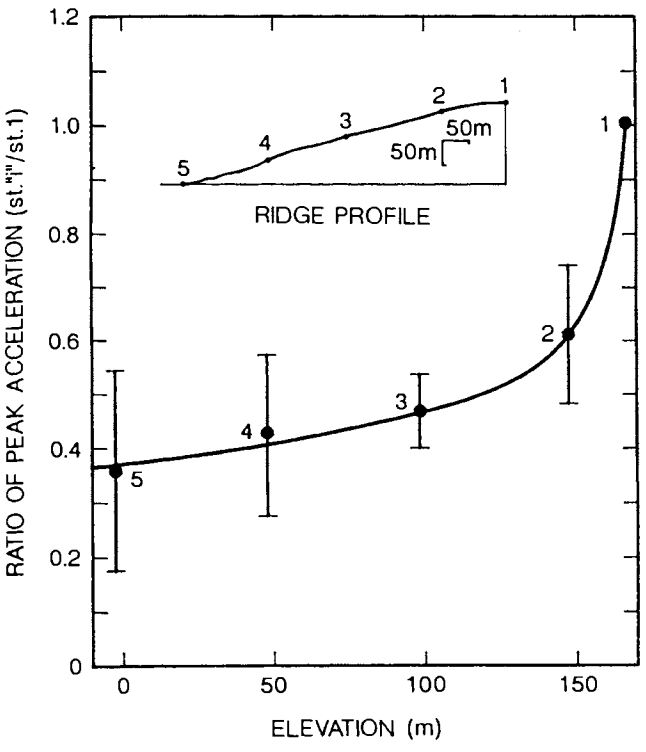

Fig.14. Peak accelerations recorded on a mountain ridge (see inset) by 5 stations of the Matsuzaki array, Japan, plotted as function of station elevation. The data are normalized by the values recorded at station 1; the curve, with the standard deviation bars, is the average for 5 earthquakes. After Jibson (1987).

SELECTING REFERENCE MOTIONS ON HARD GROUND

In hazard mapping studies or in soil response analyses, the key step of assigning reference motions on hard ground is usually affected by uncertainties arising from the lack of local accelerograph data. A conservative measure of the spread in peak values is provided by the s.e. of the prediction of current attenuation relations (typically a factor of 2 for peak acceleration). A difficulty somehow opposite in nature may arise in heavily instrumented areas, where many recordings are available. In the valley of Mexico example of Fig. 1, what are the most appropriate reference motions to be chosen for site response analyses from among the variety of recordings obtained on nominally hard ground conditions?

Volcanic areas, such as those of most capital cities in Central America, pose special difficulties in defining "bedrock", because a surficial crust of hard material (corresponding to the most recent lava flows from nearby volcanoes) frequently overlies more deformable sediments or loose deposits of volcanic ash, and the sequence may be repeated to considerable depths (Faccioli et al., 1989a).

The example illustrated below suggests that the difficulties may be caused more by the variability of frequency content than of peak values. In a recent study of nonlinear effects on the seismic response of clay in the valley of Mexico by Ordaz and Faccioli (1990), three horizontal acceleration components recorded at stations TY (Tacubaya), II and 18 (see Fig. 1) during the earthquake of 25.4.89 were first considered as input for 1D response analyses.

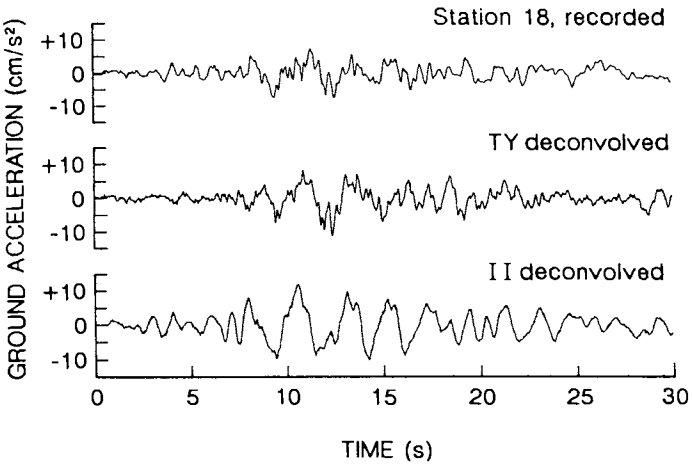

Fig.15. Portions of acceleration time histories containing the strong initial phase of motion recorded at different hard ground stations in the Mexico valley during the 25.04.89 earthquake (see Fig.1).

Fig. 15 shows the first 30 sec of the NS component recorded at st. 18, on volcanic rock, together with those obtained at firm ground stations II and TY. These were derived by deconvolution of recorded motions with the β velocity profiles labeled II and P14, respectively, in Fig. 16, which were both obtained by

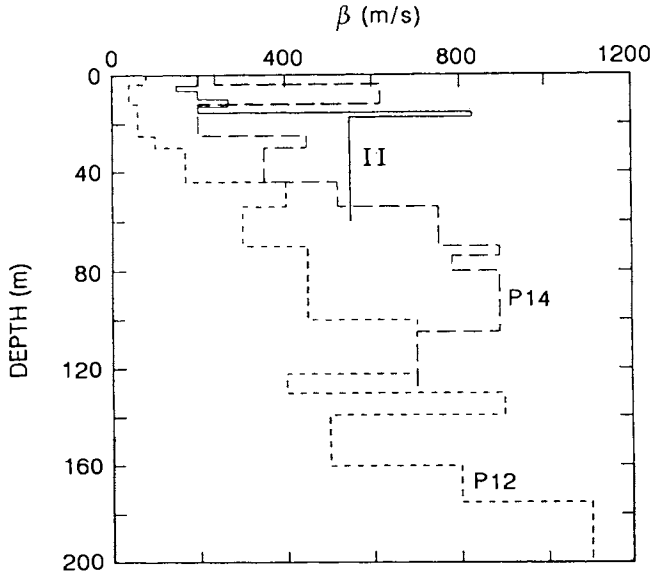

Fig.16. Profiles of S-wave velocity β measured at sites II (from Jaime, 1987), P14 and P12 (courtesy of R. Meli, Mexico City).

in-hole measurements. The deconvolution was extended to the depth were β attains about 700 m/sec at TY and about 550 m/sec at II. The analysis was limited to the initial portion of the records, as it was not intended to model the effects prominently showing up in the coda of the seismograms at the lakebed sites. The similarity of the waveforms at st. 18 and TY in the 8-to-20 sec window is worth noting. The same general characteristics of the initial strong phase are discernible also in II motions, which are, however, affected by a dominant period of about 2 s. This may be the result of some resonance phenomena occurring in the consolidated sediments which underlie the surficial crust of lava existing in the area of station II, but probably not the sites of the other two stations. Note also that the largest difference in peak-to-peak amplitude between st. 18 and II is about 30 %.

To check the validity of the deconvolved signals as input motions for further analyses, the response of st. 56 site on soft clay (see location in Fig. 1) was computed using the β profile labeled P12 in Fig. 16 and the II time-history of Fig. 15 as base excitation. The P12 shear wave velocity profile, possibly the deepest measured so far in the valley of Mexico, clearly depicts the gradual velocity increase occurring in the deep sediments formation (beginning from 45 m depth). Computed surface motions agree with the recorded ones, see Fig. 17, up to about 20 sec.

The crucial tests were carried out for the st. TD site, in the southernmost part of the valley; the measured β profile is shown by the dotted line in Fig. 18 while that used in computations is shown by the solid line. St. TD recorded the M_s8.1, great Michoacán earthquake of 19.9.85, as did stations TY and II. Deconvolution of recorded surface motions, as previously described, was carried out at TY and

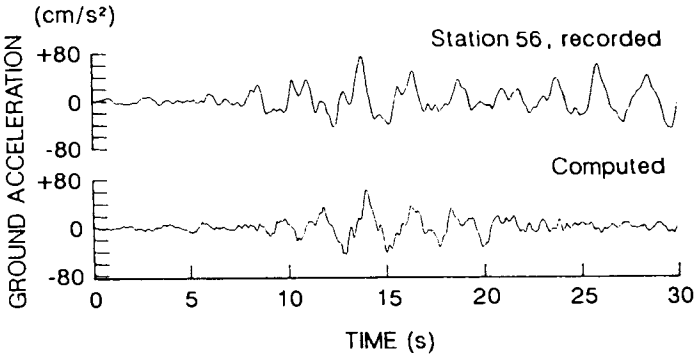

Fig.17. Computed and recorded horizontal ground acceleration at station 56, lakebed zone (see Fig.1), with reference to the strong initial phase. From Ordaz and Faccioli (1990).

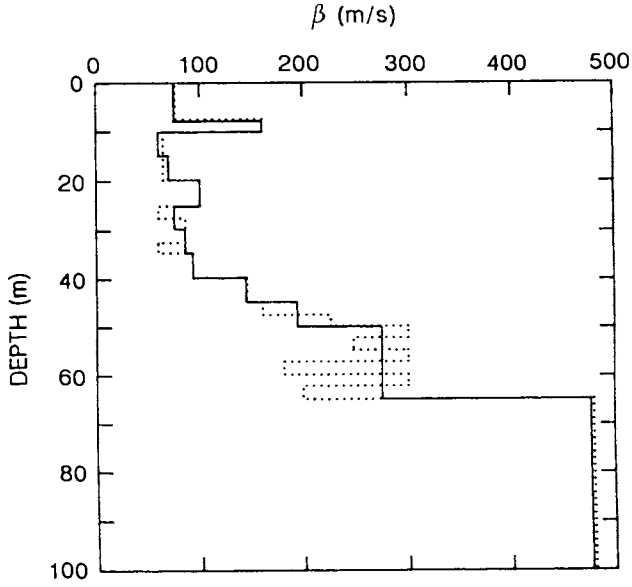

Fig.18. Profile of S-wave velocity β at site of accelerograph station TD (see Fig.1). After Jaime (1987).

II also for this earthquake, and the resulting motions were used as an input to compute the soil response at TD.

The elastic response spectrum from the calculated motion is compared in Fig. 19 with the observed one, and the difference between using TY and II as an input is immediately apparent: in the crucial period range between 1.5 and 2.5 sec the calculated spectral ordinate for TY excitation is low by a factor of up to 4 with respect to the observed one, while II motion approximately provides the correct spectral ordinate. Unless the observed motion at TD is completely controlled by 2D and 3D effects, which does not seem to be the case since the observed dominant period is compatible with 1D amplification, the results suggest that the clay layer at TD is underlain by the same deep sediment formation as site II. In this forma-

tion some resonance effects occur causing a concentration of energy in a narrow frequency band centered around 2 sec, as illustrated by the bottom waveform in Fig. 15.
It may be concluded that the definition of appropriate hard ground conditions in some areas requires that the geometry of the relevant formations be known to considerable depth.

CALCULATING THE SEISMIC RESPONSE OF NEAR-SURFACE IRREGULARITIES BY THE FOURIER (OR "PSEUDOSPECTRAL") METHOD

Main features of the method

Among numerical methods for viscoelastic wave propagation in heterogeneous media, the Fourier (or "pseudospectral") method has a strong potential in terms of efficiency, versatility and simplicity of implementation which has been only very partially exploited in earthquake engineering applications. It was originally introduced by Kosloff and Baysal (1982) as a tool for the class of geophysical problems referred to as "forward modeling", i.e. the calculation of synthetic seismograms in heterogeneous media due to explosive point sources. This usually involves no irregular free surface and a higher frequency band than in earthquake engineering problems. The first systematic applications of the method to site effect problems of interest for geotechnical earthquake engineering, containing irregular free-surface geometries and strong material heterogeneities are due to Paolucci (1989) and Faccioli et al. (1989). Because of the relative novelty of the method for the engineering community, I shall first illustrate its main features and then discuss aspects crucial for applications, concerning the treatment of boundary conditions and of incident earthquake waves.
The two-dimensional heterogeneous SH-wave equation in the absence of body forces is considered for simplicity, namely

$$\partial_x(G\partial_x v) + \partial_z (G\partial_z v) = \rho\, \partial_{tt} v \qquad (7)$$

where $G(x,z)$ and $\rho(x,z)$ are the shear modulus and density, respectively, $v(x,z)$ is the horizontal displacement in the y-direction (out-of-plane), t is time and ∂_x denotes partial derivative with respect to x. Eq. (7) can be rewritten as

$$L^2 v = \partial_{tt} v \qquad (8)$$

with L^2 a linear spatial operator given by

$$L^2 v \equiv \rho^{-1} [\partial_x(G\partial_x) + \partial_z (G\partial_z)] \qquad (9)$$

The Fourier method commonly uses an explicit second-order finite difference approximation for the time derivative of (7); staggered time grids for displacement and velocity are in this respect convenient for improving numerical stability. After introducing the velocity $V = \dot{v}$ and discretizing the time variable by $t = n\,\Delta t$, where Δt is time step size and n a natural number, (8) can be rewritten as

$$v^{n+\frac{1}{2}} = v^{n-\frac{1}{2}} + \Delta t\, L^2 v^n \qquad (10)$$

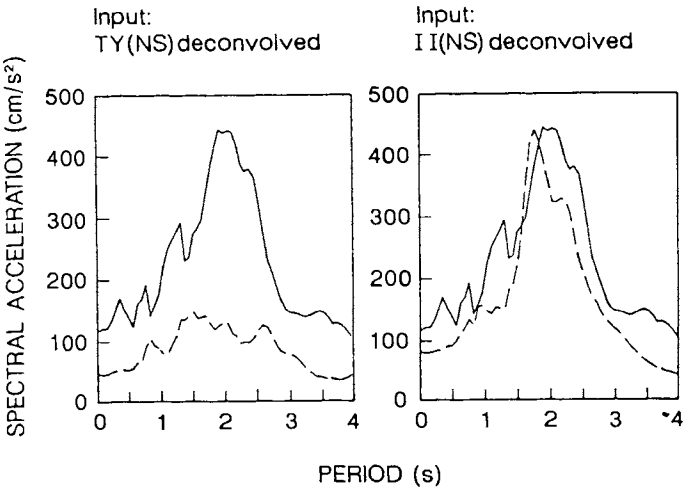

Fig.19. Influence of the choice of input motions for 1D amplification analysis on the calculated response spectrum at site TD (dashed curve), and comparison with the observed spectrum for the great earthquake of 19.09.85 (solid curve). After Ordaz and Faccioli (1990).

and

$$v^{n+1} = v^n + \Delta t\, v^{n+\frac{1}{2}} \qquad (11)$$

where the superscript represents the time coordinate.

The spatial derivatives in (10) are calculated by the Fourier method, i.e. by multiplication in the spatial wavenumber domain. Let the 2D region of analysis be replaced by a rectangular grid of M by N points and mesh sizes Δx, Δy (Fig. 20a).

The quantity $L^2 v^n$ in (10) is calculated in two separate passes, one for the term containing x-derivatives and one for that containing y-derivatives. In the first pass, the x-derivative term is calculated on all the grid lines parallel to x-direction (horizontal). Along each of these lines $\partial_x v$ is first obtained by:

a) performing a discrete Fourier Transform on v, or

$$\tilde{v}(k_m) = \Delta x \sum_{r=0}^{M-1} v(r\Delta x)\, e^{-j2\pi \frac{rm}{M}} \qquad (12)$$

where $k_m = m/M\Delta x$ $(m = 0,\ldots,M-1)$ is the spatial wavenumber vector and $j = \sqrt{-1}$;

b) multiplying the results by $j2\pi k_m$, and

c) performing the inverse transform back to space domain.

In (12), $\tilde{v}(k_m)$ denotes the transformed displacement.
In the second stage of the first pass $\partial_x v$ is multiplied by G, and again a direct and inverse transform are carried out to compute $\partial_x(G\partial_x v)$.

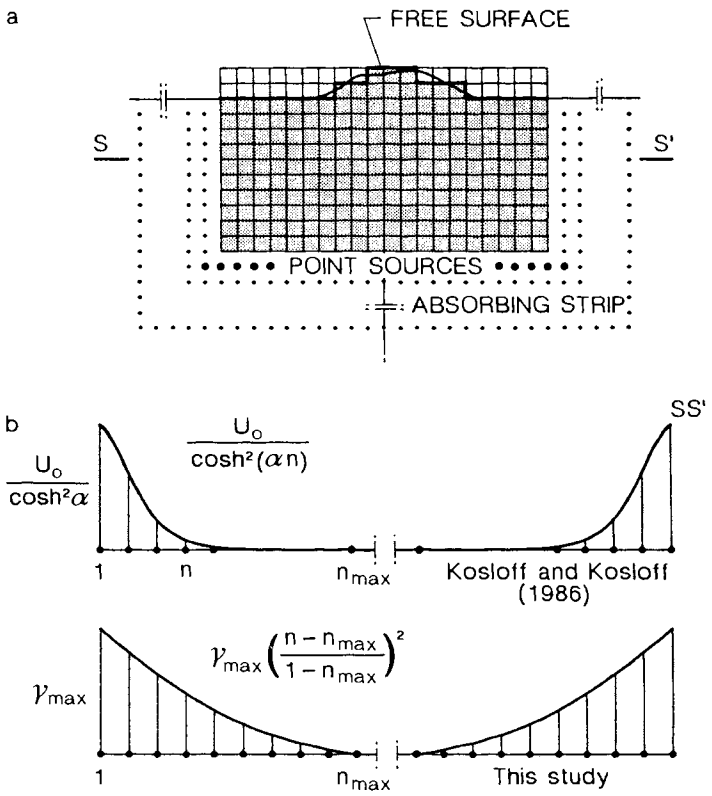

Fig.20. (a) 2D computational grid used in the pseudospectral method; (b) different distributions of parameter γ across the width of an absorbing strip.

When the calculation is completed on all horizontal lines of the grid, the same procedure is performed in a secon pass to get $\partial_z(G\partial_z v)$ on all lines in the z-direction (vertical).

The main assets of the method are that:

- The discrete Fourier transforms are efficiently performed by the FFT algorithm, which is now available in versions programmed for vectorial computers and for bases other than 2 (Temperton, 1983); these options are apt to drastically reduce computing time in 2D problems.
- The calculation of space derivatives involves a large number of points (i.e. the whole grid) allowing an acceptable solution even for media with strong jumps of material properties (Dablain, 1986). Contrasts up to a factor of 8 in the values of β of adjacent layers have been used in response analyses for the Mexico clays, similar to the example of Fig. 7, which would represent a prohibitive condition for other numerical methods such as FE and finite differences (FD).
- It is extremely efficient in terms of grid requirements, since as few as two points per wavelength in space are theoretically required by the Nyquist condition to prevent aliasing (at least in homogeneous unbounded media). A correct interpretation of this condition requires that the Nyquist frequency f_N be taken very close to the highest frequency f_c contained in the seismic excitation band, and that the grid steps satistfy the restriction

$$\max(\Delta x, \Delta y) \leq \beta_{min}/2\, f_N \qquad (13)$$

where β_{min} is the minimum velocity in the region modeled. If $f_N < f_c$, aliasing will distort the propagated signal, and the more so largest the difference $f_c - f_N$ (Brigham, 1974).
- Any noticeable grid dispersion errors produced by the Fourier method derive from the time derivative approximation, since spatial derivatives are infinitely accurate if the spatial frequencies of the signal are in the band of the mesh (Kosloff and Baysal, 1982).

For inhomogeneous and bounded media, numerical experiments have shown that 3 to 4 grid points are needed to resolve f_c, depending on the material properties and the geometry (Paolucci, cit.; Witte and Richards, 1986). With 2 points per wavelength, the method requires 25 times less grid points than the second-order explicit FD scheme, althoug it must use a smaller time step. With an explicit second-order approximation for the time derivative, a value $p = \beta_{max}\,\Delta t/\Delta x \leq 0.2$ is typically needed, as opposed to p = 0.7 for the equivalent FD method. Even so the improvement in efficiency with respect to the latter is remarkable: for a given test problem the Fourier method requires one-third the CPU time an 1/20 the computer storage (Daudt et al., 1989).

Absorbing boundaries

As is the case for most numerical methods, successful application of the Fourier method requires great care in the treatment of the boundary conditions; in addition to correctly approximating the physical conditions of earth regions, these must be suitably designed and, in a sense, created to fit the characteristics of the method. Thus, the boundaries of the grid should eliminate not only spurious edge reflections but also "wrap-around" signals, i.e. repetitions, generated by the spatial periodicity of the method. This is achieved by including along the lateral and bottom boundaries of the grid an absorbing strip, whose properties must be chosen so as to simultaneously minimize both the reflection and the transmission coefficients, R and T. To this end, the propagation equation (8) is modified into

$$L^2 v = \partial_{tt} v + 2\gamma\, \partial_t v + \gamma^2 v \qquad (14)$$

where $\gamma(x,y)$ is an absorption parameter which differs from zero only in the aforementioned strip (Kosloff and Kosloff, 1986). For 1D propagation in a homogeneous medium, the solution to (14) is a wave traveling without dispersion, and with amplitude decreasing exponentially with distance at a frequency independent rate γ/β, so that a pulse will gradually attenuate without changing shape.

In the absorbing strip, the integration scheme (10) can be replaced by

$$v^{n+\frac{1}{2}} = [v^{n-\frac{1}{2}}(1-\gamma\Delta t)+\Delta t L^2 v^n - \gamma^2 v^n]/(1+\gamma\Delta t) \quad (15)$$

while (11) remains unchanged.

Different forms for the functional dependence of γ on the distance from the boundary are used to optimize the efficiency of the absorbing strip in the sense previously explained. At the extremes of low and high frequencies, all forms are affected by a strong frequency-dependence of R. In earthquake response analyses, minimizing the value of R at the lower end of the frequency band of interest, i.e. significantly below 1 Hz, may pose some problems.

Kosloff and Kosloff (1986) have shown how to compute numerically R and T for any given frequency and for an arbitrary spatial dependence of γ; their preference is for the following expression

$$\gamma_n = U_0/\cosh^2(an) \qquad n=1,\ldots n_{max} \quad (16)$$

where U_0 = constant, a = decay factor, n =distance in number of grid points from the boundary, and n_{max} = width of the absorbing strip. Eq. (16), illustrated in Fig. 20, is a good choice for the frequency band of geophysical exploration, i.e. above a few Hz: an optimal set of parameter values in this range is n_{max} = 18, a = 0.11 m^{-1} and U_0= 0.35 $\beta_{max}/\min(\Delta x,\Delta y)$, where β_{max} is the largest propagation velocity in the mesh (Carcione, 1990). Numerical experiments have shown, however, that the ability of (16) to generate assigned target values for R and T in a specified range of frequencies is more difficult to predict than that of other forms, because the function and its first two derivatives are strongly nonlinear. As an alternative, both linear and quadratic variations of γ (Fig. 20b) have been tested; the latter, i.e.

$$\gamma_n = \gamma_{max}[(n-n_{max})/(1-n_{max})]^2 \quad n=1,..n_{max} \quad (17)$$

where γ_{max} is the value of γ prescribed on the boundary, possesses some desirable properties over the frequency band of interest. Specifically, it has been verified that, for a given Δx or Δy:

- the transmission coefficient T varies but weakly with frequency and depends only on the area under the curve (17), i.e. on the quantity

$$A = \left\{ \begin{array}{c} \Delta x \\ \Delta z \end{array} \right\} \sum_{n=1}^{n_{max}} \gamma_n \quad (18)$$

  which is proportional to the product b = $\gamma_{max}\, n_{max}$.
- the curve describing the reflection coefficient R as a function of frequency depends only on the second derivative, or "curvature" of eq. (17), i.e. the constant quantity

$$c = \gamma_{max}/n_{max}^2 . \quad (19)$$

Figs. 21 and 22 contain some numerically calculated curves illustrating the properties in question, and useful as a guidance in practical applications; in Fig. 21 the intermediate group of nearly coinciding curves corresponds to different combination of γ_{max} and n_{max} yielding the same value of b (γ_{max} = 15, 7.5, 5 and n_{max}= 30, 60, 90 respectively). In Fig.22, displaying the behavior at low frequencies of the reflection coefficient R, the lowest group of nearly coinciding curves corresponds to different combinations of γ_{max} and n_{max} yielding the same value of c (γ_{max} = 9, 36, 81 and n_{max}= 30, 60, 90 respectively). Note that for a fixed n_{max} and frequency, T decreases with increasing γ_{max} while R does the opposite, so that some preliminary numerical testing should be carried out to find optimal values of n_{max} and γ_{max} for problems involving significant frequency components below about 1.5 Hz. In principle, n_{max} should be such that the width of the strip is of the order of the significant wavelength to be analyzed if displacement histories free of low frequency noise are needed. However, if one is mainly interested in accelerations, about 30 grid points are typically sufficient.

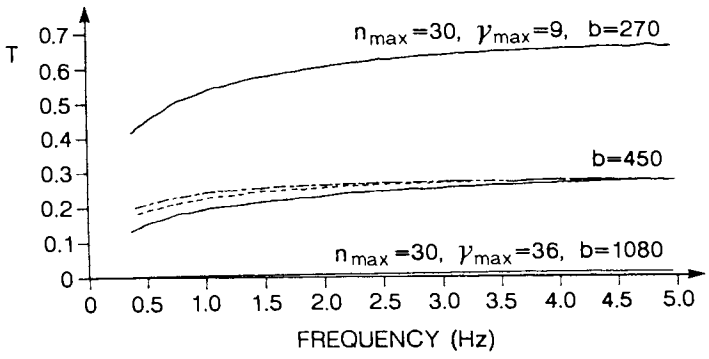

Fig.21. Transmission coefficient T of absorbing strip with quadratic variation of γ: influence of γ_{max} and n_{max}.

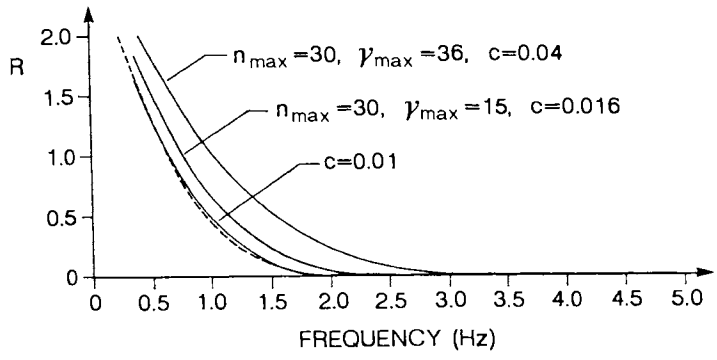

Fig.22. Reflection coefficient R of absorbing strip with quadratic variation of γ: influence of γ_{max} and n_{max}.

Earthquake excitation

The numerical calculation of response to a prescribed earthquake excitation can be initiated either by an initial condition, or by source functions. The former requires a given spatial distribution of displacement and velocity at zero time and, therefore, additional grid points. On the other hand, if point sources are used, the excitation is input at the base of the model via a row of grid points just above the bottom section of the absorbing strip (Fig. 20a), without introducing a rigid base. For horizontally incident waves, the point sources are on a column adjacent to the lateral absorbing strips.

At each point source a displacement, or velocity, is introduced having the prescribed temporal dependence and duration. As long as the excitation acts, the calculated displacement (or velocity) at this point is added to the imposed one at the end of each time step. In addition to being computationally convenient, the point source procedure allows for great flexibility, because plane waves with non-normal incidence are easily handled by shifting the onset of excitation at each source point by a constant interval, compatible with the apparent velocity of the traveling wave. More complex types of incident wavefronts can be treated by simply assigning different displacement histories to different source points. Note that a point source is the product of a time function by a discrete delta function in space; the latter, by itself, would cause aliasing of the wavenumbers beyond the Nyquist value $\pi/\Delta x$. However, if the time function of the source is band limited with cutoff frequency f_c, the wavenumbers larger than $2\pi f_c/\beta$ are automatically filtered so that the incident wave can be propagated without distorsion. When several seismograms are to be obtained for different source time functions with the same numerical model, it is convenient to compute first the numerical Green's function. This procedure will save substantial computing time because the Green's function is simply the response of the given model to a numerical impulsive source (or line of point sources, if plane waves are treated); and it can be calculated once for all. Convolution of such response with the source time functions will then yield the synthetics at the desired receiver points.

To obtain the Green's function one can use as an input a smoothed delta function with a flat Fourier spectrum over a prescribed frequency band or, more economically, the space delta function $1/\Delta x$ applied for a single time step at the source point(s). As previously pointed out, this will produce an aliased Green's function but the inconvenient will be remedied by subsequent convolution with a bandlimited source time function.

Free-surface and material interfaces

A non trivial problem of the Fourier method is the treatment of the earth surface with sufficient numerical accuracy. Because of the staircase approximation of any irregular free surface imposed by the grid discretization (Fig.20a), the condition of vanishing normal stress translates into having vanishing spatial derivatives of the displacement in the x- and/or in the z- direction at the grid points on the surface. According to Kosloff et al. (1984), the traction-free boundary condition on a horizontal surface can be achieved by the "zero padding" technique, i.e. by simply including a wide zone in the lower portion of the grid containing zero values for the material constants, which also has the beneficial effect of removing periodicity in the vertical direction. The results, however, are not satisfactory due to non-causal disturbances and low frequency distorsions affecting the calculated response at surface points.

Numerical tests by Paolucci (cit.) and Tagliani (1989) have shown that a significant improvement results from the introduction of additional rows of grid points beyond the free surface, and by adopting the following procedure:

- The displacement value, $\bar{v}$, calculated at a surface point is imposed at about 10 grid points beyond the surface (in the direction normal to it);
- By using a sinusoidal taper over an additional distance of about 20 grid points, the displacement is decreased from the value $\bar{v}$ to zero at the grid boundary (so that a total of about 30 grid point must be introduced beyond the free-surface);
- At the point on the surface, the additional condition $\partial_x v=0$) is imposed.

The first condition alone would cause the numerically computed derivative to vanish only starting from the first grid point beyond the surface, so that on the surface point itself a strong jump in the derivative would occur. To avoid this, the third condition is introduced. Finally, sinusoidal tapering is widely adopted in the Fourier analysis of discrete time series. Even by the previous procedure some slight numerical errors persist in the form of phase delays; by propagating a simple double impulse in a homogeneous half-space and by checking the zero-crossing arrival, it has been verified that a time delay approximately equal to $\Delta x/4\beta$ (or $\Delta z/4\beta$) occurs. The reason is that the jump in material properties introduced by a free surface is equivalent to a step function in space, and in order to correctly resolve such a function one would need a vanishing grid step since its Fourier spectrum goes to zero only for infinite wavenumbers. The accuracy of the previous free-surface procedure was also tested in the frequency domain by computing the surface response/excitation spectral ratio for a homogeneous half-space. It has been verified that the frequency range where the free-surface amplification factor of 2 is accurately reproduced does not depend on the frequency content of the incident wave, but only on the grid step size, as illustrated in Fig.23. This shows that a numerically accurate free-surface condition may require a smaller grid step than the Nyquist condition, depending on the frequency band of interest. As an example, surface synthetics cannot be accurately computed for frequencies larger than about 6-7 Hz unless $\Delta x \leq 20$m.

Numerical techniques capable of accounting for the free surface without introducing errors require a non uniform grid spacing and may thus not be compatible with the Fourier method.

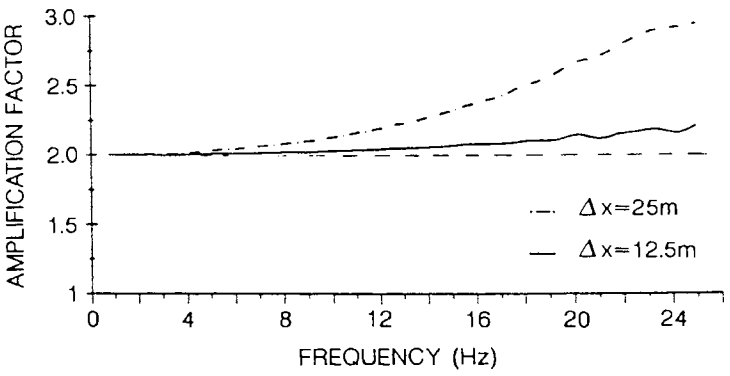

Fig.23. Free-surface amplification factor as a function of frequency and grid step size, calculated by 1D model. From Paolucci (1989).

The presence of discontinuities in the material properties, such as a horizontal interface between two plane layers, introduces a time delay error similar to the free surface. Specifically, for a wave travelling from a medium with velocity β_2 into another medium with velocity β_1, the arrival of the refracted wave is anticipated by an amount $(\beta_2^{-1} - \beta_1^{-1})$ $\Delta x/2$ while the reflected wave is retarded by an amount $\Delta x/\beta_1$. The errors are negligible for moderate velocity contrasts and/or for complex layered structures in which the phase errors tend to compensate, but can lead to grossly inaccurate results in the case of a single layer over a half-space in which the successive reflections within the layer produce an accumulation of errors. If such a case were analyzed by a 1D model, with n grid points corresponding to the layer thickness H, the previous error can be corrected by taking Δx such that

$$H + (\Delta x/4) - (\Delta x/2) = n\,\Delta x, \qquad (20)$$

or $\Delta x = H/(n - \frac{1}{4})$.

Internal damping

Internal damping in geomaterials is preferably assumed as hysteretic, so that the damping coefficient ξ, or the intrinsic quality factor $Q^i = 1/2\xi$, must be frequency-independent. The result can be achieved by the use of multiple absorption mechanisms that are combined to produce frequency-independent absorption over a desired frequency range (Emmerich and Korn, 1987). This causes, however, a significant increase in storage requirements and in computing time. An alternative approach has been devised by Faccioli and Tagliani (1989), theoretically less satisfactory but practically useful. Its main feature is the introduction of a complex propagation velocity or, equivalently, of a complex shear modulus

$$G^* = G_o\,(1 + \frac{j}{Q}) \qquad (21)$$

which causes the displacement v and the propagation equation (7) to become complex. The solution is carried out by splitting (7) into a real and an imaginary part, and by an appropriate modification of the source time function which suppresses the negative frequency components of its spectrum. This method gives rise to non-dispersive, acausal propagation and to numerical instability, but the errors are negligible for the range of propagation distances of interest, provided values of $Q^i \geq 40 - 50$ are used.

Examples

To evaluate the accuracy of the Fourier method in problems of the type illustrated in Figs.7 and 8, several tests were conducted on 2D models previously solved by other methods.

A first example is the triangular canyon in a homogeneous half space (Fig.24), for which two angles of incident were analyzed, i.e. $\theta = 0°$ and 45°. Parameter values actually used in the computation are a = 200 m/s, $\Delta h = \Delta x = \Delta z = 25$ m, $\Delta t = 0.001$ sec, while $\beta = 2500$ m/s was assumed for the homogeneous half-space. An incident wave consisting of a double impulse with a duration of about 0.2 sec. and a spectral peak at about 8 Hz was used. The Nyquist condition would be satisfied with a grid step Δh as large as 35 m, since the frequency cutoff of the excitation is about 35 Hz, but this would produce unacceptable errors at the surface. The computation was carried out on a grid of 128x64 points (no absorbing strip was found necessary) over 600 time steps, or 0.6 sec., requiring about 10 min CPU time on a IBM 3090 system with vectorial facility. A second run was also performed with one-half the previous values of Δh and Δt. Synthetic seismograms were calculated at evenly spaced receivers on the surface; frequency domain results were obtained by Fourier transforming the synthetics and computing the ratio with respect to the input spectrum. Fig.25 depicts

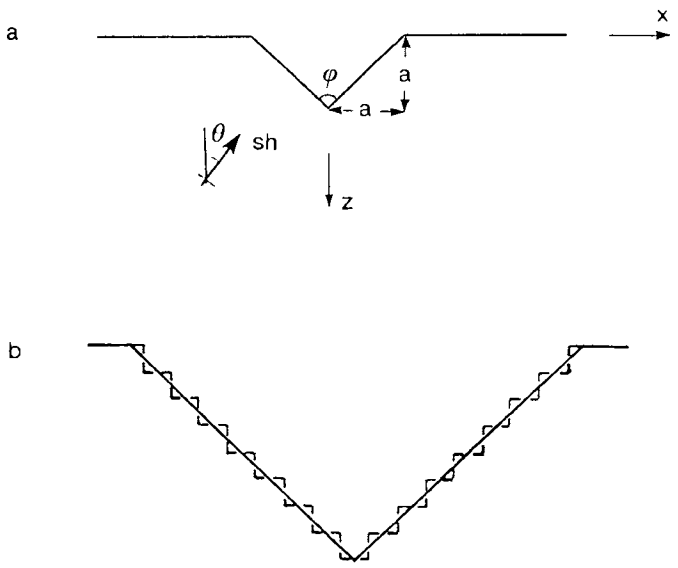

Fig.24. Triangular canyon with $\phi = 90°$ at the surface of homogeneous half-space, and its "staircase" discretization by a grid step $\Delta h = a/8$.

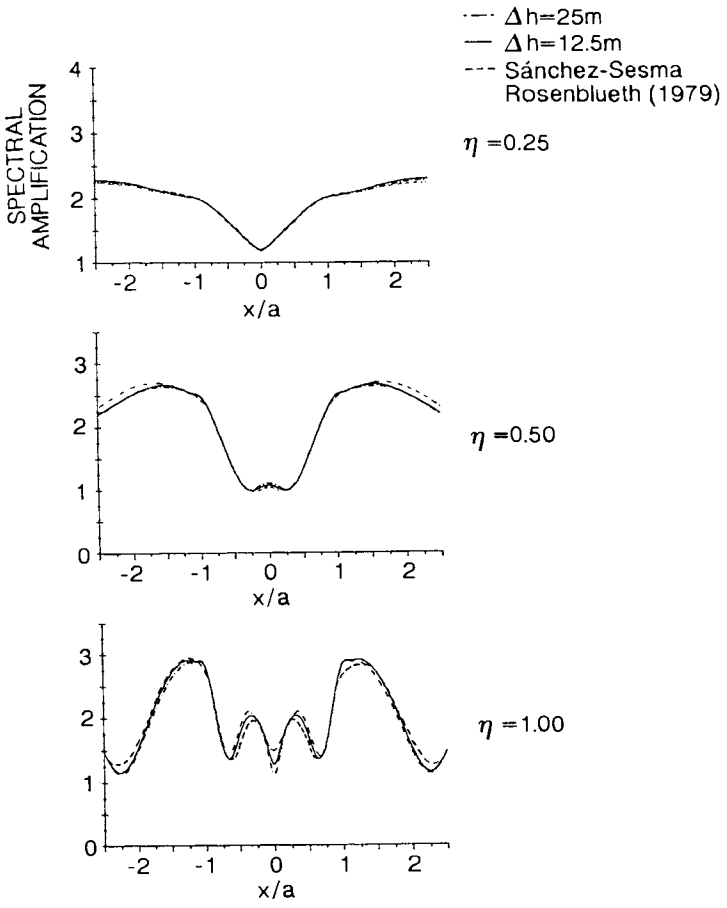

Fig.25. Spectral amplification on the surface of triangular canyon for vertically incident SH waves and different values of the normalized frequency $\eta = 2af/\beta$. Illustrated is the influence of the grid step on the results and a previous solution by Sánchez-Sesma and Rosenblueth (1979), shown by dotted line. From Paolucci (1989).

the distribution of spectral amplification at the surface in the case $\theta = 0°$ for different values of the non-dimensional frequency $\eta = 2af/\beta$, corresponding to f = 1.56, 3.12 and 6.25 Hz. For both values of the grid step size (25m and 12.5m) the results closely agree with the solution by Sánchez-Sesma and Rosenblueth (1979); the larger discrepancies for $\eta = 1$ are the likely result of a stronger influence of the "staircase" approximation of the canyon profile at high frequency. The ensemble of surface synthetics in Fig.26 clearly shows the generation of Love waves by the corners of the canyon.

The analysis for oblique incidence, i.e. $\theta = 45°$, was carried out with the same numerical parameters (Δh = 12.5m) but a larger array of 256x256 grid points in order to include a lateral absorbing strip 80 grid points wide. The accuracy of the results is checked also in this case with the solution by Sánchez-Sesma and Rosenblueth, as shown in Fig.27. The agreement between solutions deteriorates somewhat for $\eta = 1.0$, but this is mostly the result of

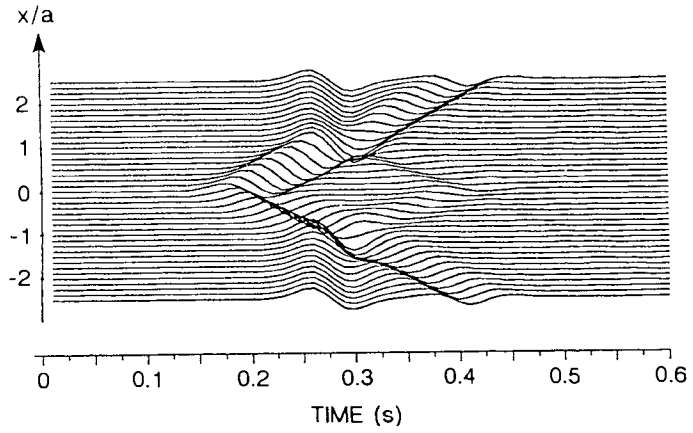

Fig.26. Time histories of the responses calculated along the surface of triangular canyon for vertical incidence. From Paolucci (1989).

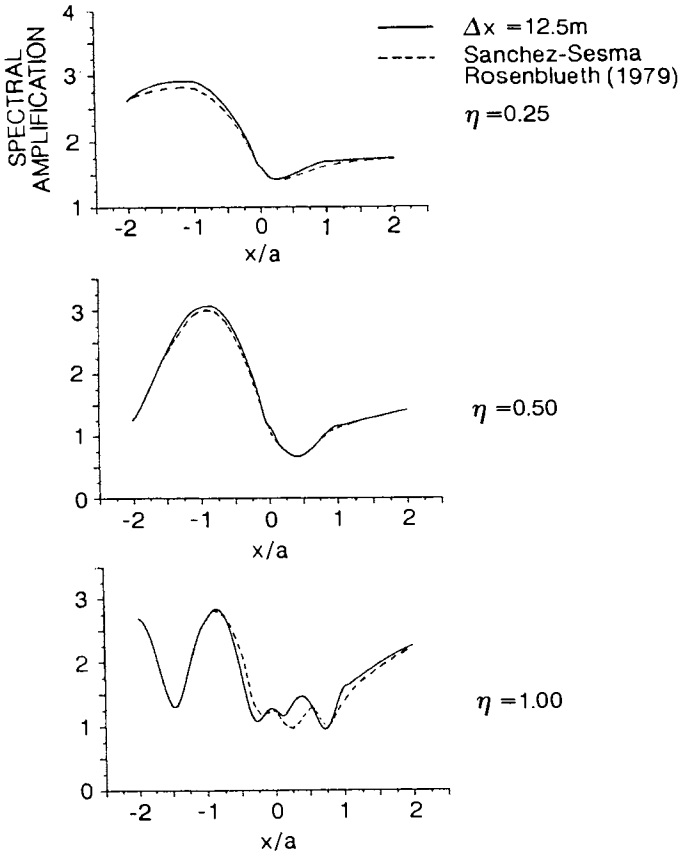

Fig.27. As in Fig.25, but for $\theta = 45°$.

the different geometrical approximations adopted for the bottom vertex of the canyon. In the Sánchez-Sesma and Rosenblueth solution this is in fact smoothed by a segment of circumference. In Fig.27, the factor of 3 difference in amplification at the surface points x/a = +1 and -1 for $\eta = 0.5$ is worth noting.

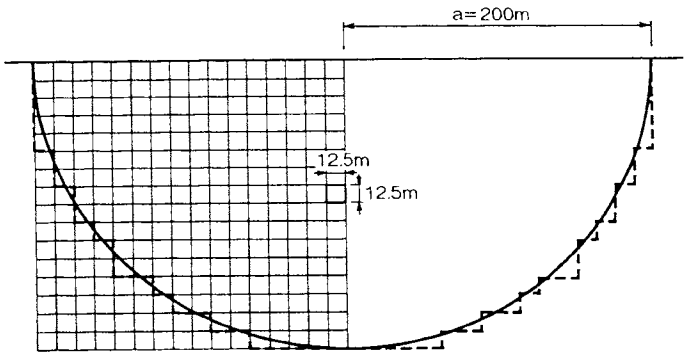

Fig.28. Semicircular alluvial valley in a homogeneous half-space, with geometrical approximation used in calculations.

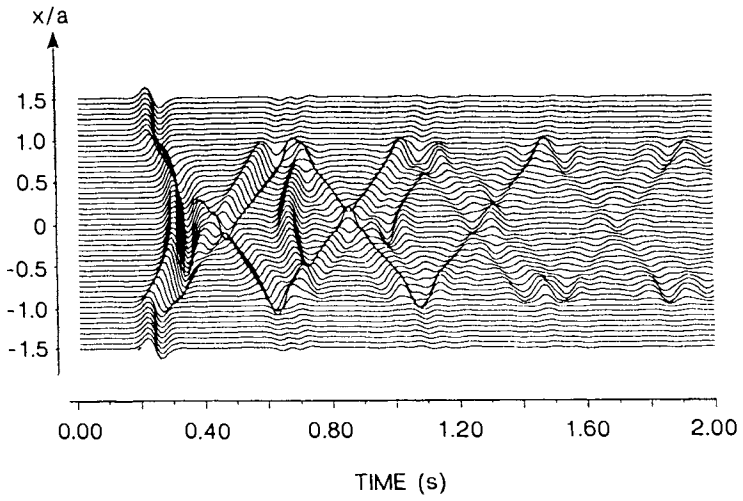

Fig.29. Time histories of the responses calculated along the surface of inhomogeneous, semicircular alluvial valley (of radius a) and nearby zones for vertical incidence. From Paolucci (1989).

A further instructive example for the illustration of site effects is the seismic response of a semicircular deposit of radius a (Fig.28), filled by a material with shear modulus G^R linearly increasing with depth, i.e.

$$G^R(z)/G^E = G_o + G_1 (z/a), \quad 0 \le z \le a \qquad (22)$$

where G^E = shear modulus of surrounding half space, G_o = 0.0833 and G_1 = 0.1666. The density ratio ρ^R/ρ^E is constant and equal to 2/3, and the propagation velocity in the half-space is β^E = 2500 m/s. The same values of Δh and Δt and the same input as in the previous example were adopted, with an array of 128x256 point and 5000 time steps, requiring about 75 min CPU time on the vectorial IBM 3090 system.

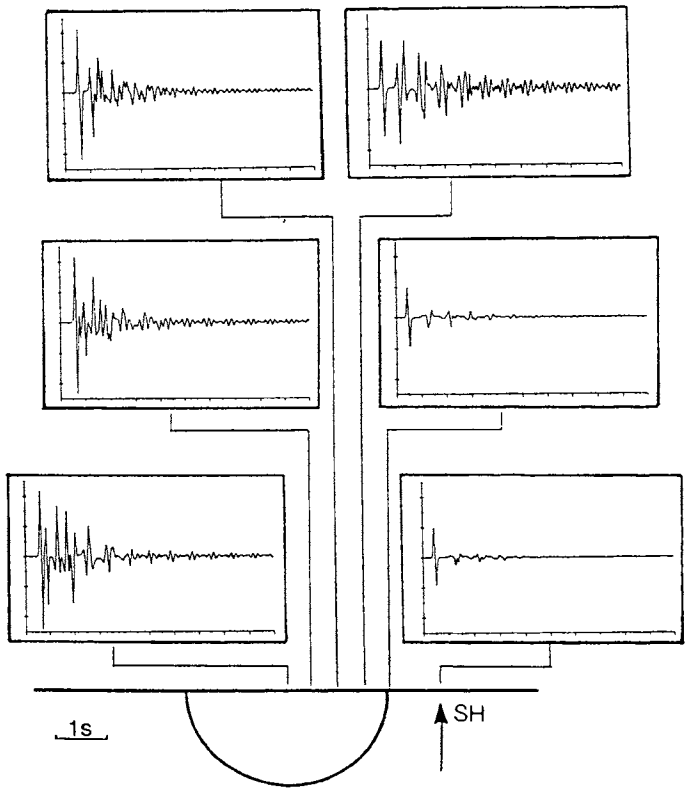

Fig.30. Complete synthetics at selected receivers on the surface of semicircular alluvial valley. From Paolucci (1989).

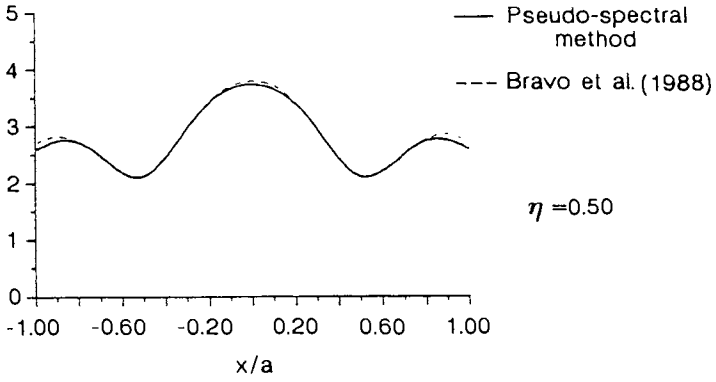

Fig.31. Spectral amplification on the surface of semicircular alluvial valley for given value of normalized frequency $\eta = 2af/\beta$; comparison of present method (solid line) with previous solution, shown by dashed line, by Bravo et al. (1988). From Paolucci (1989).

The synthetics at 49 surface receivers evenly spaced by 12.5m are displayed for a 2 sec time window in Fig.29, while the complete ground motions at selected points on the deposit and the adjacent half space are given in fig.30. Note the complexity, the amount of amplification and the increase in significant duration of motions at the surface of the deposit, in contrast to the simplicity and short duration of the inci-

dent pulse. These effects are mainly due to the efficient generation and propagation of Love waves within the deposit, and are obviously enhanced by the lack of internal dissipation. The accuracy of the present solution can be checked by the spectral amplification values at the surface calculated through a different method by Bravo et al. (1988), as illustrated in Fig.31. These authors report only the result for $\eta = 0.5$, for which the agreement is very good.

CONCLUSIONS

In the first part of this paper I have illustrated the role of several crucial factors in the evaluation of site effects on earthquake ground motions, drawing both on the evidence contained in recent instrumental data of high quality, and on the indications provided by numerical and analytical solutions to some illustrative model problems. Simple exact solutions for elementary geometries, such as the wedge-shaped mountain or the infinite horizontal soil wedge, can prove quite useful in design problems, as well as in interpreting the pecularities of experimental observations and in estimating the right order of magnitude of local amplification. For cases in which this cannot be done, there seems to be a need for relatively simple and flexible computational methods, at least for viscoelastic soil behavior, that can be implemented in most cases directly by the designer without recurring to expensive and complex computer codes.

In such a perspective, the second part of the paper illustrates the Fourier (or pseudo-spectral) method for the time-domain numerical analysis of wave propagation in heterogeneous viscoelastic media. The method's strongest asset lies in the calculation of space derivatives, which absorbs most of the computational time, and is very efficiently performed by the FFT technique, today available also in versions appropriate for vectorial computers. Originated and widely used in the field of exploration geophysics, the Fourier method is not very familiar yet to engineering seismologists and earthquake geotechnical engineers. For this reason, I have dwelt in some detail on its characteristics and especially on aspects of its application requiring special care, such as the choice of absorbing boundaries and the treatment of a free surface. Most of the results presented in this context are original, in the sense that the writer and his associates were probably the first to systematically explore the application of the method to typical problems of earthquake site effects analysis. The selected examples hopefully provide a valid indication on the potential of this approach, but significant work remains to be done, such as the extension to P-SV wave propagation including a sufficiently accurate treatment of a free surface.

In conclusion, as I have hinted upon in the Introduction, I believe that recent developments do not call for substantial changes in the main conclusions of Aki's (1988) review of the present subject. However, further light is needed on some of the key problems involved (e.g. 2D vs. 1D models, choice of motions on reference ground) and an enlargement of the computational tools would be desirable and beneficial.

ACKNOWLEDGMENTS

The cooperation of C. Battistella (Studio Geotecnico Italiano, Milano) in performing the calculations behind Figs. 11, 21, 22 and in pre-processing the graphic material for Figs.1 and 4, as well as of S. Bacci for preparing the figures is gratefully acknowledged. The 2D wedge calculations for Figs. 10, 11, 13 are due to R. Paolucci, who also critically reviewed parts of the manuscript. I am also indebted to M. Fachin and F. Rocca for typing the manuscript.
The Mexican accelerograph data were kindly provided by M. Ordaz. F. Sánchez-Sesma revised the whole manuscript and gave valuable suggestions.
The research was partly supported by the National Research Council of Italy (CNR - Gruppo Nazionale Difesa Terremoti).

REFERENCES

Aki, K. (1988), "Local Site Effects on Strong Ground Motion", in J. Lawrence Van Thun (Ed.), "Earthquake Engineering and Soil Dynamic II - Recent Advances in Ground-Motion Evaluation", pp.103-155, Park City, Utah, U.S.A.

Bard, P.Y., M. Campillo, F. Chávez García and F. Sánchez-Sesma (1988), "A Theoretical Investigation of Large and Small-scale Amplification Effects in the Mexico City Valley", Earthquake Spectra, 4, pp.609-634.

Bravo, M.A., F. Sánchez-Sesma and F. Chávez García (1988), "Ground Motion and Stratified Alluvial Deposits for Incident SH Waves", B.S.S.A., 78, pp.436-450.

Brigham, E. (1974), "The Fast Fourier Transform", Prentice-Hall Inc., Englewood Cliffs, New Jersey, U.S.A.

Caillot, V., and P.Y. Bard (1990), "Characterizing Site Effects for Earthquake Regulations in the French Seismicity Context: a Statistical Analysis", presented at CEE (Eurocode 8) Workshop on "Seismic Input Data", Lisbon, Portugal, 2-3 July.

Carcione, J. (1990), Personal communication.

Chávez García, F. and P.Y. Bard (1989), "Effect of Random Thickness Variations on the Seismic Response of a Soft Soil Layer: Applications to Mexico City", in A. Cakmak and I. Herrera (eds.), "Engineering Seismology and Site Response" pp.247-261, CM Publications, Southampton, England.

Dablain, M. (1986), "The Application of High-Order Differencing to the Scalar Wave Equation", Geophysics, 51, pp.54-66.

Daudt, C., L. Braile, R. Nowack and C. Chiang (1989), "A Comparison of Finite-Difference and Fourier Method Calculations of Synthetic Seismograms", B.S.S.A., 79, pp.1210-1230.

Emmerich, H. and M. Korn (1987), "Incorporation of Attenuation into Time-Domain Computations of Seismic Wave Fields", Geophysics, 52, pp.1252-1264.

Faccioli, E. and Reséndiz, D. (1976), "Soil Dynamics: Behavior Including Liquefaction"

in "Seismic Risk and Engineering Decisions", C. Lomnitz and E. Rosenblueth (Eds.), pp.71-139, Elsevier, Amsterdam, The Netherlands.

Faccioli, E. and A. Tagliani (1989), "A Time Domain Approach to Seismic Propagation in Randomly Inhomogeneous Media with Constant Q", in G. Carlomagno and C. Brebbia (Eds.) "Computers and Experiments in Stress Analysis", pp.99-114, Proc. 4th Int. Conf. on Computational Methods and Experimental Measurements, Capri, Italy, May 1989. CML Publications, Southampton.

Faccioli, E., C. Battistella, P. Alemani, D. Lo Presti and A. Tibaldi (1989a), "Seismic Microzoning and Soil Dynamics Studies in San Salvador", in "Earthquake Geotechnical Enginneering", Proc. of Discussion Session on Influence of Local Conditions on Seismic Response, pp.21-36, XII I.C.S.M.F.E., Rio de Janeiro, Brazil.

Faccioli, E., A. Tagliani and R. Paolucci (1989b), "Effects of Wave Propagation in Random Earth Media on the Seismic Radiation Spectrum", in A. Cakmak and I. Herrera (Eds.), "Structural Dynamics and Soil-Structure Interaction", pp.61-75, CM Publications, Southampton, England.

Jaime, P. (1987), "Características Dinámicas de la Arcilla del Valle de México", Doctoral Thesis, Faculty of Engineering, Universidad Nacional Autónoma de México, Mexico City.

Jarpe, S., L. Hutchings, T. Hauk and A. Shakal (1989), "Selected Strong- and Weak-Motion Data from the Loma Prieta Earthquake Sequence", Seismol. Res. Letters, 60, pp.167-176.

Jibson, R. (1987), "Summary of Research on the Effects of Topographic Amplification of Earthquake Shaking on Slope Stability", U.S. Geological Survey Open-File Report 87-268, Menlo Park, California, U.S.A.

Kjartansson, E. (1979), "Constant Q-Wave Propagation and Attenuation", J. Geophys. Res., 84, pp.4737-4748.

Kosloff, D. and E. Baysal (1982), "Forward Modeling by a Fourier Method", Geophysics, 47, pp.1402-1412.

Kosloff, D., M. Reshef and D. Loewenthal (1984), "Elastic Wave Calculations by the Fourier Method", B.S.S.A., 74, PP.875-891.

Kosloff, R. and D. Kosloff (1986), "Absorbing Boundaries for Wave Propagation Problems", J. Comp. Phys., 63, pp.363-376.

Ohta, T., S. Hiehata, K. Takahashi, E. Kitamura, M. Motosaka, M. Kamata and M. Miyamura (1986), "Research on the Strong Ground Motion in Mexico City During the Earthquake of September 19, 1985 Michoacán-Guerrero, Mexico", Report n.68, Kajima Institute of Construction Technology, Tokyo.

Ordaz, M. and E. Faccioli (1990), "A Study of Nonlinear Soil Response in the Valley of Mexico", submitted for publication.

Paolucci, R. (1989), "Il Metodo Pseudo-Spettrale nella Soluzione di Problemi di Calcolo della Risposta Sismica Locale", Thesis for the Degree of Civil Engineering, Technical University of Milan, Milan, Italy, (in Italian).

PWRI (Public Works Research Institute) (1986), "Dense Instrument Array Observation of Strong Earthquake Motion", Ministry of Construction, Tsukubo, Japan.

Sánchez-Sesma, F. (1990), "Elementary Solutions for Response of a Wedge-Shaped Medium to Incident SH and SV Waves", B.S.S.A., 80, pp.737-742.

Sánchez-Sesma, F. and E. Rosenblueth (1979), "Ground Motion at Canyons of Arbitrary Shape under Incident SH Waves", Earth. Eng. Struct. Dynam., 7, pp.441-450.

Sánchez-Sesma, F., E. Faccioli and R. Fregonese (1986), "An Index for Measuring the Effects of Topography on Seismic Ground Motion Intensity", Earth. Eng. Struc. Dynam., 14, pp.719-731.

Sánchez-Sesma, F., S. Chávez, M. Suárez, M. Bravo and L. Pérez (1988a), "On the Seismic Response of the Valley of Mexico", Earthquake Spectra, 4, pp.569-590.

Sánchez-Sesma, F., F. Chávez García and M. Bravo (1988b), "Seismic Response of a Class of Alluvial Valleys for Incident SH Waves", B.S.S.A., 78, pp.83-95.

Seed, H., H. Romo, J. Sun, A. Jaime and Lysmer (1988), "The Mexico Earthquake of September 19, 1985 - Relationship Between Soil Conditions and Earthquake Ground Motions", Earthquake Spectra, 4 (4), pp.687-729.

Singh, S., E. Mena and R. Castro (1988), " Some Aspects of Source Characteristics of the 19 September 1985 Michoacán Earthquake and Ground Motion Amplification In and Near Mexico City from Strong Motion Data", B.S.S.A., 78, pp.451-477.

Tagliani, A. (1989), "Effetti della Propagazione di Onde Sismiche negli Strati Superficiali della Crosta Terrestre", Proc. 4th National Conference "L'Ingegneria Sismica in Italia", pp.244-253, Pàtron Editore, Bologna, Italy (in Italian).

Temperton, C. (1983), "Fast Mixed Radix Real Fourier Transforms", J. Comp. Phys., 52, pp.340-350.

Tokida, K. (1989), Written Personal Communication.

Witte, D. and P. Richards (1986), "Anelastic Wave Propagation by the Pseudo-Spectral Method", EOS Transactions, 67, p.303.